Electronic Supplementary Material (ESI) for Journal of Materials Chemistry A.

Nanoporous trimetallic PdCuAg alloys as efficient electrocatalysts by all-direction accessibility and synergetic effects

Jun-Xuan Li,[a] Hong-Xing Yin,[b] Qinghong Geng,[a] Dawei Du,[a] Lian Ma,[a] Longlong Fan,[a] Qingfeng Hua[a] and Cuiling Li*[a]

[a] Key Laboratory of Cluster Science, Ministry of Education, Beijing Key Laboratory of Photoelectronic/Electrophotonic Conversion Materials, School of Chemistry and Chemical Engineering, Beijing Institute of Technology, Beijing 100081, China

[b] Analysis & Testing Center, Beijing Institute of Technology, Beijing 100081, China

E-mail: licuiling@bit.edu.cn

Experimental Procedures

Chemicals. Sodium tetrachloropalladate (Na_2PdCl_4), Pluronic P123 and F127, L-ascorbic acid (AA), commercial palladium black (PdB) nanoparticles, Nafion solution (5 wt% in alcohol and H_2O) were purchased from Sigma Aldrich. 1,3,5-trimethyl benzene (TMB), copper(II) chloride dehydrate ($CuCl_2 \cdot 2H_2O$), potassium hydroxide (KOH) were purchased from J&K Scientific Ltd. (Beijing, China). Silver nitrate ($AgNO_3$) and hydrochloric acid (HCl) were obtained from Xilong Chemical Industry Co., Ltd. (Sichuan, China).

Characterization. A field emission scanning electron microscope (SEM, Zeiss Supra 55, Zeiss, Germany) operating at 20 kV was used to observe the morphology of PdCuAg nanoparticles. Transmission electron microscopy (TEM), high-angle annular dark field (HAADF) images, and energy-dispersive X-ray (EDX) mapping were observed with a FEI, Talos F200X apparatus (Thermo Fisher, the United States) at an accelerating voltage of 200 kV. X-ray diffraction (XRD) characterization was carried recorded on Ultima IV X-ray diffractometer (Rigaku, Japan) at a scanning rate of 1.5 degrees per min with a Cu-Ka radiation (40 kV, 40 mA) source. X-ray photoelectron spectroscopy (XPS) analysis was conducted on PHI 5000 Versaprobe III scanning microprobe multi-functional X-ray photoelectron spectroscopy (ULVAC-PHI, Japan). ICP-MS and ICP-OES were recorded on Aglient 7800 and Aglient 5110 spectrometer (Agilent Technologies, the United States), respectively.

Synthesis of nanoporous PdCuAg nanoparticles. The nanoporous PdCuAg nanoparticles were prepared via a swollen agent-merging-micelles approach. In a typical synthesis, 5 mg of P123, 15 mg of F127, and 10 μL of TMB were first dissolved in 1.4 mL of mixed H_2O/ethanol solution (volume ratio of 2:5) under ultrasonication to form the swollen agent-merging micelle solution, followed by the addition of 50 μL of HCl (1 M HCl for $d_{71}Cu_{27}Ag_2$ and $Pd_{68}Cu_{26}Ag_{11}$, 5 M HCl for $Pd_{66}Cu_{23}Ag_{11}$ and

$Pd_{64}Cu_{22}Ag_{14}$). Then, 0.4 mL of 40 mM H_2PdCl_4, 0.2 mL of 40 mM $CuCl_2$ and certain amount of 40 mM $AgNO_3$, were successively added, and the molar ratio of $[PdCl_4]^{2-}$:Cu^{2+}:Ag^+ in the mixed solution was controlled to be 65:33:2 to 63:31:6, 57:29:14 and 53:27:20. Subsequently, 0.5 mL of freshly prepared 200 mM ascorbic acid solution was injected. The mixed solution was further incubated at 90 ℃ for 10 h to yield a dark black solution. Finally, the samples were collected by centrifugation at 8000 rpm for 8 min, followed by consecutive washing/centrifugation cycles with ethanol.

Electrochemical Measurements. Electrochemical measurements were measured using a CHI 760E electrochemical analyzer (Chenhua Instrument Company, China). The three-electrode cell consisted of saturated calomel electrode (SCE) as the reference electrode, Pt wire as the counter electrode and glassy carbon electrode (GCE) modified by the catalysts as the working electrode. 1 mg of the as-obtained catalyst was ultrasonically dispersed in 1 mL ultrapure Milli-Q water (18.2 MΩ·cm) to form the catalyst ink. Then, 5 μL of the suspension was dropped onto the surface of the GCE. After the electrode was dried under ambient temperature, 2 μL of Nafion ethanol solution (0.05 vol%) was then dropped onto the catalysts. The electrode was air-dried for further electrochemical measurements. The ethanol oxidation reaction (EOR) measurement was carried out in the electrolyte containing 1 M C_2H_5OH and 1 M NaOH.

Product Detection: The EOR product analysis mainly focused on the carbonate (C1 product) and acetate (C2 product). For quantifying the liquid products, the electrolyte after chronoamperometric measurements at indicated potentials for 0.5 h was collected and analyzed by ^{1}H nuclear magnetic resonance (^{1}H-NMR) and Ion Chromatography, respectively. For ^{1}H-NMR analysis, 0.5 mL of electrolyte was mixed with 0.1 mL of D_2O (DMSO concentration of 100 ppm). The Ion Chromatograph was equipped with 930 Compact IC flex and 919 autosampler plus. Separations were done on a Metrosep organic Acid-250/7.8 chromatographic column, coupled with a Metrosep RP2 Guard column. The 0.5 mM H_2SO_4 and 100 mM LiCl solutions were used as eluent and regenerant, respectively. An intelligent conductivity detector with a chemical suppressor (MSM) was used for detection. Calibration standards (formic acid and acetic

acid) were prepared in a series of concentrations, and the linear correlation coefficient was >99.9%. In the case of ion chromatography detection, 5.0 mL of electrolyte was diluted with 5.0 mL H_2O. After the quantification, the faradaic efficiency (FE) of the products were calculated as follows:

$$\text{FE (\%)} = \frac{amount\ of\ product \times n \times F}{C} \times 100\%$$

where n is number of moles of electrons to participate in the faradaic reaction, F is the Faraday constant (96485 C mol^{-1}), and C is the amount of charge passed through the working electrode.

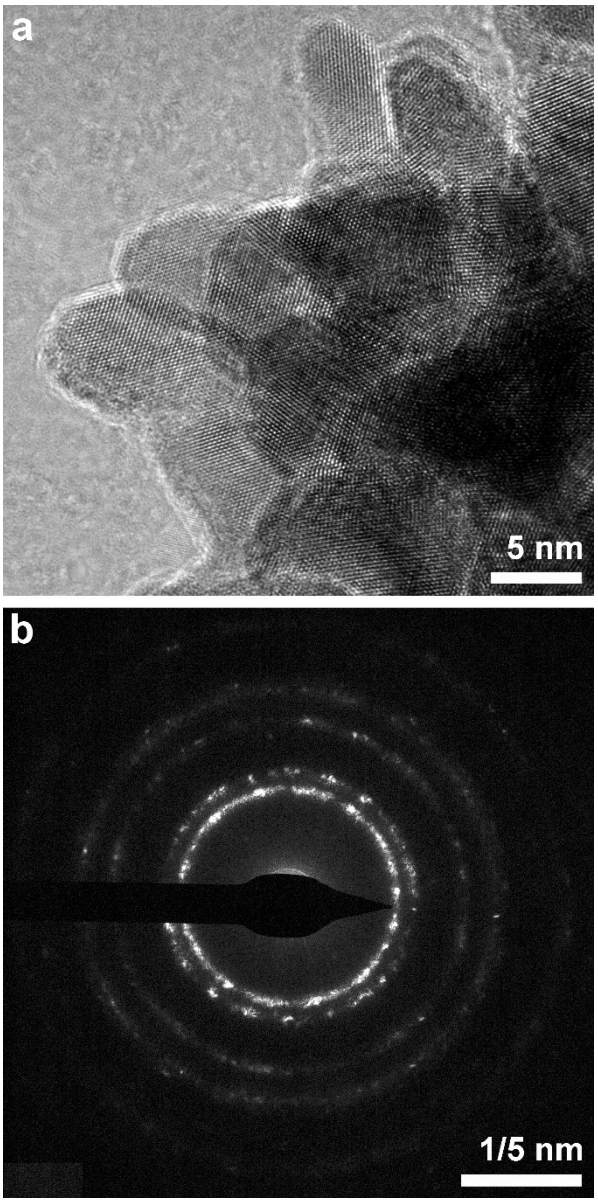

Fig. S1 (a) HRTEM image of the edge of one nanoporous $Pd_{68}Cu_{26}Ag_6$ nanoparticle and (b) SAED derived from one nanoporous $Pd_{68}Cu_{26}Ag_6$ nanoparticle. Both results reveal the polycrystallinity of the products.

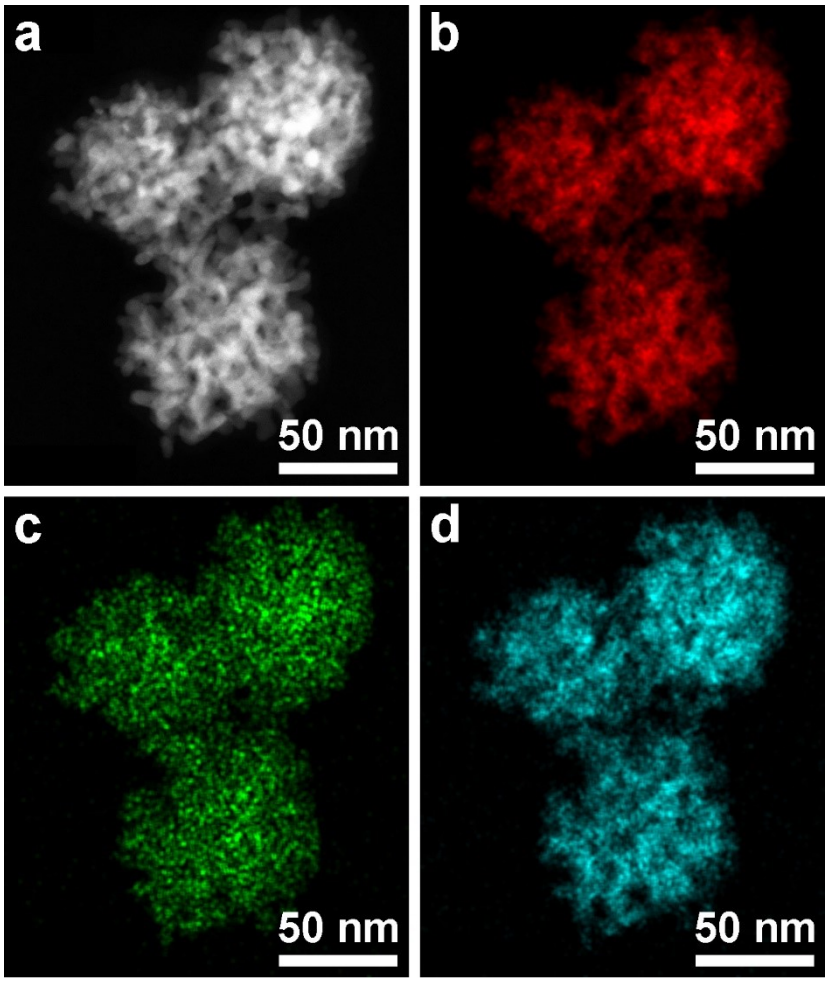

Fig. S2 (a) HAADF-STEM image and corresponding elemental maps ((b) Pd, (c) Cu and (d) Ag) of nanoporous $Pd_{71}Cu_{27}Ag_2$ nanoparticles.

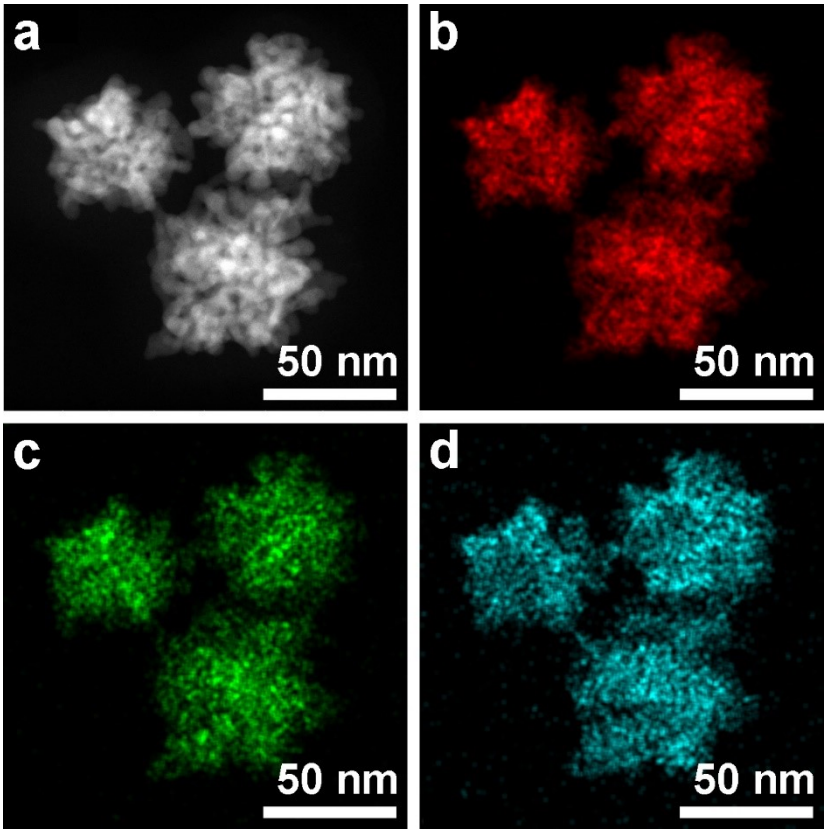

Fig. S3 (a) HAADF-STEM image and corresponding elemental maps ((b) Pd, (c) Cu and (d) Ag) of nanoporous $Pd_{66}Cu_{23}Ag_{11}$ nanoparticles.

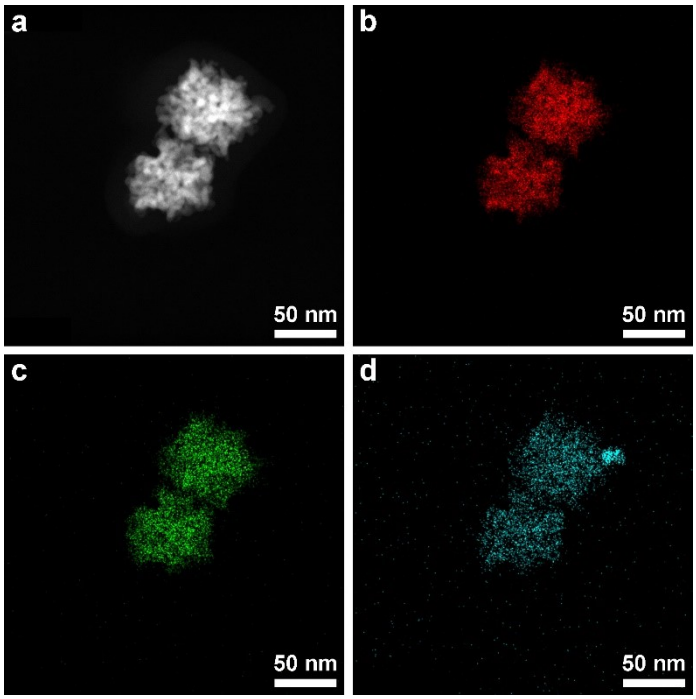

Fig. S4 (a) HAADF-STEM image and corresponding elemental maps ((b) Pd, (c) Cu and (d) Ag) of nanoporous $Pd_{64}Cu_{22}Ag_{14}$ nanoparticles.

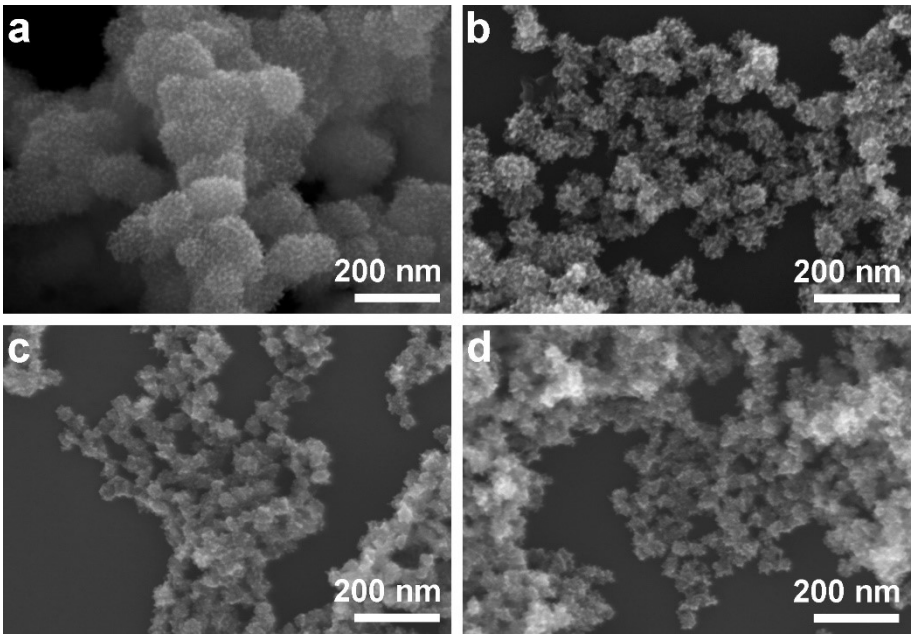

Fig. S5 Typical SEM images of the nanoporous $Pd_{68}Cu_{26}Ag_6$ nanoparticles by changing the TMB amounts: (a) 0 μL, (b) 10 μL, (c) 20 μL and (d) 50 μL, respectively.

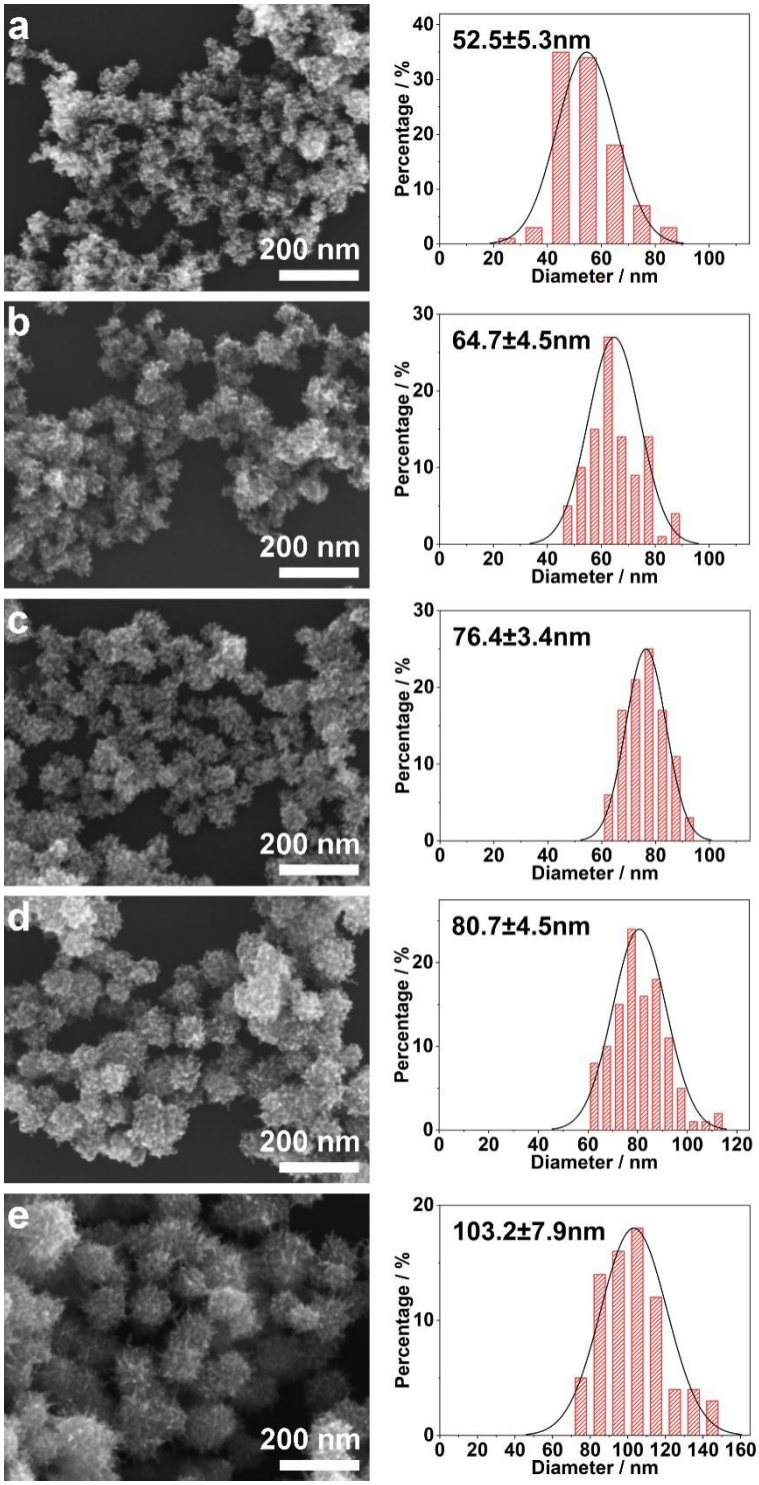

Fig. S6 Typical SEM images of the nanoporous $Pd_{68}Cu_{26}Ag_6$ nanoparticles by changing the HCl concentrations: (a) 3.9 mM, (b) 9.6 mM, (c) 19.3 mM, (d) 57.7 mM and (e) 96.2 mM, respectively. The histograms on the right side show the distributions of the corresponding particle sizes.

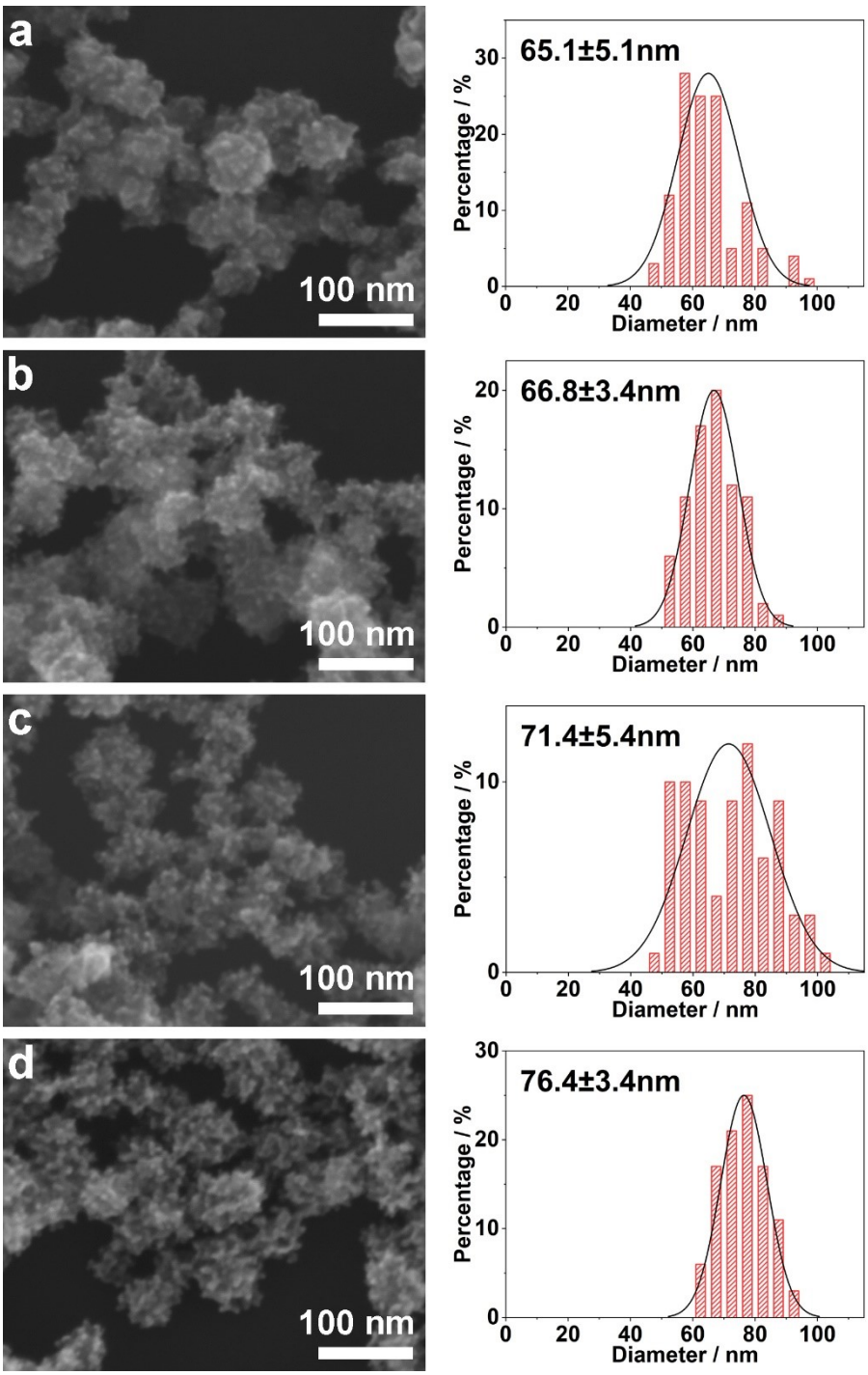

Fig. S7 Typical SEM images of the products collected at different reaction times: (a) 5 min, (b) 20 min, (c) 5 h and (d) 10 h, respectively. The histograms on the right side show the distributions of the corresponding particle sizes.

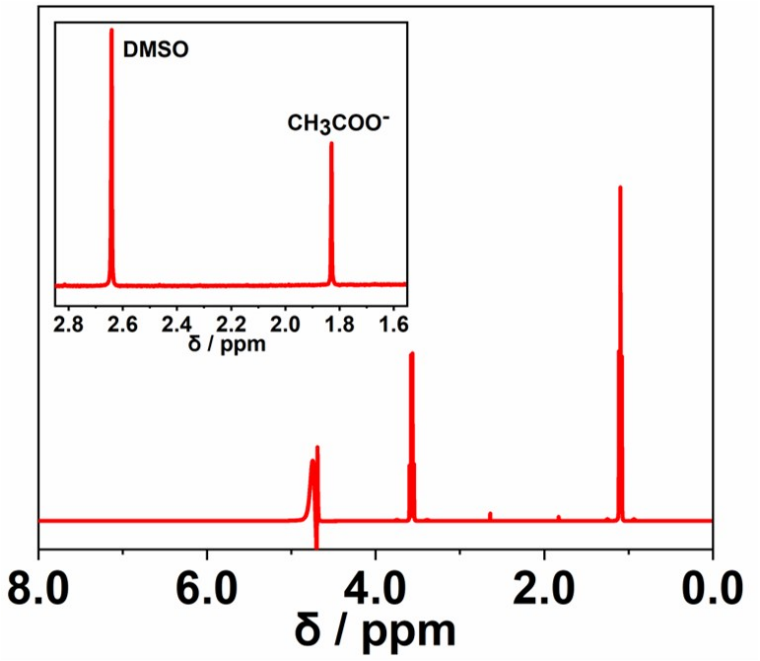

Fig. S8 Representative ^{1}H-NMR spectra of the electrolyte after EOR catalyzed by $Pd_{68}Cu_{26}Ag_6$ nanoparticles at -0.3 V *vs.* SCE for 0.5 h. DMSO is used as an internal standard for quantification of CH_3COO^- and $HCOO^-$.

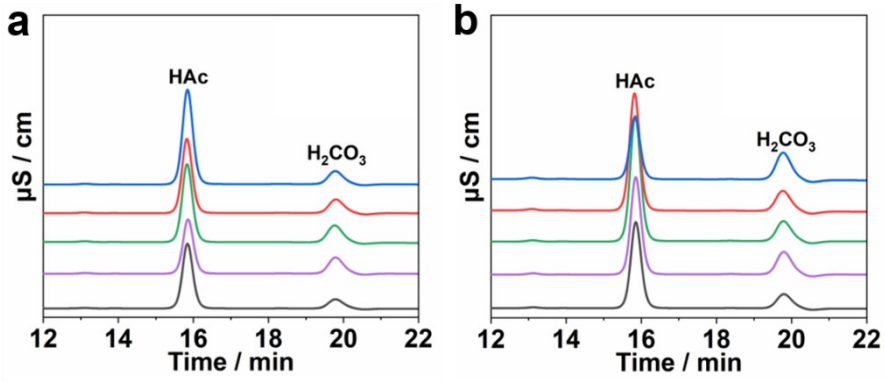

Fig. S9 Representative ion chromatographic spectra of the electrolyte after EOR catalyzed by $Pd_{71}Cu_{27}Ag_2$ (blue), $Pd_{68}Cu_{26}Ag_6$ (red), $Pd_{66}Cu_{23}Ag_{11}$ (green), $Pd_{64}Cu_{22}Ag_{14}$ (purple) and PdB (black) at (a) -0.2 V *vs.* SCE and (b) -0.3 V *vs.* SCE for 0.5 h.

Table S1 Summary of the metal compositions and size parameters of the final products.

Samples	Molar ratio of Pd:Cu:Ag in the precursors	Molar ratio of Pd:Cu:Ag in the products	Surface mole percentage of Pd confirmed by XPS (%)	Average particle size (nm)	Grain size (nm)
$Pd_{71}Cu_{27}Ag_2$	65:33:2	71:27:2	84	81.3±4.2	7.9
$Pd_{68}Cu_{26}Ag_6$	63:31:6	68:26:6	76	76.4±3.4	7.5
$Pd_{66}Cu_{23}Ag_{11}$	57:29:14	66:23:11	72	60.9±4.6	6.7
$Pd_{64}Cu_{22}Ag_{14}$	53:27:20	64:22:14	70	50.0±4.7	6.5

Table S2 A summary of the EOR activity on Pd-based electrocatalysts in alkaline solution.

Electrocatalyst	Electrolyte	Scan rate (mV s^{-1})	Mass activity (A mg^{-1}_Pd)	Reference
$Pd_{68}Cu_{26}Ag_6$	**1 M KOH +1 M C_2H_5OH**	**50**	**4.04**	**This work**
$Pd_1Cu_{1.2}$ nanocages	1 M KOH +1 M C_2H_5OH	50	1.79	S1
Pd_2Ag_1 single-crystalline nanowires	1 M KOH +1 M C_2H_5OH	50	2.84	S2
PdAg nanodendrites	1 M KOH +1 M C_2H_5OH	50	2.60	S3
C-PdSn/SnO_x	1 M KOH +1 M C_2H_5OH	50	3.2	S4
Au@Pd Nanorods	1 M KOH +1 M C_2H_5OH	50	2.92	S5
PdNi particle networks	1 M KOH +1 M C_2H_5OH	50	2.4	S6
$Pd_{21}Cu_{79}$	0.5 M KOH +0.5 M C_2H_5OH	50	1.78	S7
$Pd_4Ir_2Ni_1$/C	1 M KOH +1 M C_2H_5OH	50	0.52	S8
PdAg hollow nanoflowers	1 M KOH +1 M C_2H_5OH	50	1.62	S9
PdAgNi/C	1 M KOH +1 M C_2H_5OH	50	2.7	S10
PdCu nanoparticles	1 M KOH +1 M C_2H_5OH	50	2.36	S11
Pd_3Sn-nanodots	1 M KOH +1 M C_2H_5OH	50	4.02	S12
PdAu 3:1/C_{-1}	0.5 M KOH +0.2 M C_2H_5OH	50	0.10	S13
Pd_7/Ru_1 nanodendrites	1 M KOH +1 M C_2H_5OH	50	~1.15	S14
Au@PdAuCu mesospheres	1 M KOH +1 M C_2H_5OH	50	3.99	S15
PdCo nanotube /carbon cloth	1 M KOH +1 M C_2H_5OH	50	~1.50	S16
CuPdNiP nanohollow structure	1 M KOH +1 M C_2H_5OH	50	1.19	S17

In_3Pd_2/C	1 M KOH +1 M C_2H_5OH	50	2.82	S18
Pd_4Au_1-P/PDIL-CNTs	1 M KOH +1 M C_2H_5OH	50	2.30	S19
Pd-$NiCoO_x$/C	0.5 M KOH +1 M C_2H_5OH	50	~0.45	S20

Table S3 Faradic efficiency for C1 or C2 reaction pathway estimated based on the IC quantification toward reaction products.

Electrocatalyst	Potential (V vs. SCE)	FE-C2 products (%)	FE-C1 products (%)
$Pd_{71}Cu_{27}Ag_2$	-0.2	95.74	4.26
	-0.3	94.00	6.00
$Pd_{68}Cu_{26}Ag_6$	-0.2	94.92	5.08
	-0.3	96.55	3.45
$Pd_{66}Cu_{23}Ag_{11}$	-0.2	97.86	2.14
	-0.3	94.51	5.49
$Pd_{64}Cu_{22}Ag_{14}$	-0.2	94.98	5.02
	-0.3	95.64	4.36
PdB	-0.2	97.78	2.22
	-0.3	97.59	2.41

REFERENCES

S1. P. Yu, H. Xu, L. Jin, C. Chen, H. Shang, Q. Liu and Y. Du, *J. Colloid Interface Sci.*, 2019, **555**, 195-202.

S2. H. Lv, Y. Wang, A. Lopes, D. Xu and B. Liu, *Appl. Catal., B*, 2019, **249**, 116-125.

S3. W. Huang, X. Kang, C. Xu, J. Zhou, J. Deng, Y. Li and S. Cheng, *Adv. Mater.*, 2018, **30**, 1706962.

S4. Q. Gao, T. Mou, S. Liu, G. Johnson, X. Han, Z. Yan, M. Ji, Q. He, S. Zhang, H. Xin and H. Zhu, *J. Mater. Chem. A*, 2020, **8**, 20931-20938.

S5. Y. Chen, Z. Fan, Z. Luo, X. Liu, Z. Lai, B. Li, Y. Zong, L. Gu and H. Zhang, *Adv. Mater.*, 2017, **29**, 1701331.

S6. J. Ding, S. Ji, H. Wang, B. G. Pollet and R. Wang, *J. Appl. Electrochem.*, 2018, **49**, 39-44.

S7. J. Yin, S. Shan, M. S. Ng, L. Yang, D. Mott, W. Fang, N. Kang, J. Luo and C. J. Zhong, *Langmuir*, 2013, **29**, 9249-9258.

S8. A. Elsheikh, H. M. Mousa and J. McGregor, *Micromachines*, 2021, **12**, 1327.

S9. D. Bin, B. Yang, K. Zhang, C. Wang, J. Wang, J. Zhong, Y. Feng, J. Guo and Y. Du, *Chem. Eur. J.*, 2016, **22**, 16642-16647.

S10. A. Elsheikh and J. McGregor, *Nanomaterials*, 2021, **11**, 2244.

S11. Y. Cheng, J. Xue, M. Yang, H. Li and P. Guo, *Inorg. Chem.*, 2020, **59**, 10611-10619.

S12. T. Song, F. Gao, Y. Zhang, P. e. Yu, C. Wang, Y. Shiraishi, S. Li, C. Wang, J. Guo and Y. Du, *J. Taiwan Inst. Chem. Eng.*, 2019, **101**, 167-176.

S13. B. Jin, Y. Zhang and L. Zhao, *J. Appl. Electrochem.*, 2016, **46**, 1147-1155.

S14. K. Zhang, D. Bin, B. Yang, C. Wang, F. Ren and Y. Du, *Nanoscale*, 2015, **7**, 12445-12451.

S15. H. Lv, L. Sun, X. Chen, D. Xu and B. Liu, *Green Chem.*, 2019, **21**, 2043-2051.

S16. A. L. Wang, X. J. He, X. F. Lu, H. Xu, Y. X. Tong and G. R. Li, *Angew. Chem. Int. Ed.*, 2015, **54**, 3669-3673.

S17. D. Chen, R.-H. Zhang, Q.-Y. Hu, Y.-F. Guo, W. Zhan, S.-N. Chen, X.-W. Zhou and Z.-X. Dai, *ACS Appl. Energy Mater.*, 2019, **2**, 5525-5533.

S18. Y. J. Chen, Y. R. Chen, C. H. Chiang, K. L. Tung, T. K. Yeh and H. Y. Tuan, *Nanoscale*, 2019, **11**, 3336-3343.

S19. H. Yang, Z. Yu, S. Li, Q. Zhang, J. Jin and J. Ma, *J. Catal.*, 2017, **353**, 256-264.

S20. W. Wang, Y. Yang, Y. Liu, Z. Zhang, W. Dong and Z. Lei, *J. Power Sources*, 2015, **273**, 631-637.